Origin of spin-driven ferroelectricity and effect of external pressure on the complex magnetism of the 6*H* perovskite Ba₃HoRu₂O₉

E. Kushwaha ⬤,[1] G. Roy ⬤,[1] M. Kumar ⬤,[1] A. M. dos Santos ⬤,[2] S. Ghosh,[1] D. T. Adroja,[3,4] V. Caignaert,[5] O. Perez,[5] A. Pautrat,[5] and T. Basu ⬤[1,*]

[1]*Department of Sciences and Humanities, Rajiv Gandhi Institute of Petroleum Technology, Jais, Amethi, 229304, India*
[2]*Neutron Scattering Division, Oak Ridge National Laboratory, Oak Ridge, Tennessee 37831, USA*
[3]*ISIS Neutron and Muon Source, STFC, Rutherford Appleton Laboratory, Chilton, Oxon OX11 0QX, United Kingdom*
[4]*Highly Correlated Matter Research Group, Physics Department, University of Johannesburg, Auckland Park 2006, South Africa*
[5]*CRISMAT Normandie Université, ENSICAEN, UNICAEN, UMR CNRS 6508, 6 Boulevard Maréchal Juin, 14050 Caen Cedex 4, France*

The compound Ba₃HoRu₂O₉ magnetically orders at 50 K (T_{N1}), followed by another complex magnetic ordering at 10.2 K (T_{N2}). The second magnetic phase transition was characterized by the coexistence of two competing magnetic ground states associated with two different magnetic wave vectors ($K_1 = 0.5\,0\,0$ and $K_2 = 0.25\,0.25\,0$). The multiferroicity and magnetoelectric coupling were predicted below T_{N2} in these $4d$-based materials. Here, we have discussed the origin of spin-driven ferroelectricity, which is not known yet, and the nature of magnetoelectric domains. We have investigated the compound through time-of-flight neutron diffraction, synchrotron x-ray diffraction (XRD), ac susceptibility, frequency-dependent complex dielectric spectroscopy, and dc magnetization under external pressure. We have demonstrated that the noncollinear structure involving two different magnetic ions, Ru ($4d$) and Ho ($4f$), breaks the spatial inversion symmetry via inverse Dzyaloshinskii-Moriya (DM) interaction through strong $4d$-$4f$ magnetic correlation, which shifts the oxygen atoms and results in nonzero polarization. Such an observation of inverse DM interaction from two different magnetic ions which cause ferroelectricity is rarely observed. The stronger spin-orbit coupling of $4d$ orbital might play a major role in creating DM interaction of noncollinear spins. We have systematically studied the spin and dipolar dynamics, which exhibit intriguing behavior with shorter coherence lengths of second magnetic phase associated with the k_2 wave vector. The results manifest the development of finite-size magnetoelectric domains instead of true long-range ordering, which justifies the experimentally obtained low value of ferroelectric polarization. The lattice parameters and volume show a sharp anomaly at T_{N2} obtained by analyzing the temperature-dependence XRD, which is consistent with the ferroelectric transition, predicting a noncentrosymmetric space group, $P\bar{6}2c$, for this compound. Furthermore, we have investigated the effect of external pressure on this complex magnetism. The result reveals an enhancement of ordering temperature by the application of external pressure ($\sim$1.6 K/GPa). The external pressure might favor stabilizing the magnetic ground state associated with second magnetic phase. Our study shows an unconventional mechanism of spin-driven ferroelectricity involving inverse DM interaction between Ru ($4d$) and Ho ($4f$) magnetic ions due to strong $4d$-$4f$ cross coupling.

I. INTRODUCTION

The multiferroic materials, in which magnetic and ferroelectric phases coexist, and where spins and electric dipoles are strongly coupled, have picked up momentum in condensed matter physics in recent years due to their future potential application in memory devices and fundamental interest [1–3]. Several systems with $3d - 4f$ coupling that show multiferroic behavior are known, with many of these widely studied: e.g., RMnO₃ [1,2], RMn₂O₅ [3–5], RCrTiO₅ [6,7], and R_2BaNiO₅ [8,9], where R is a rare earth. However, in these systems, spatial inversion symmetry breaks due to complex patterns associated with the $3d$ transition-metal ion. This

arises from the coupling of strong electronic correlations with magnetic frustration [2,10,11], specifically the antisymmetric Dzyaloshinskii–Moriya (DM) interaction [12,13], wherein noncollinear spins break spatial inversion symmetry, inducing a nonzero polarization in materials [1]; exchange-striction, at which lattice distortion is induced by the symmetric exchange interaction between neighboring magnetic ions in a material, leading to changes in the crystal structure [14], and spin-ligand interaction (spin-dependent *p-d* hybridization) where the local polar bond connecting the spin site and the ligand site can be modulated by the spin-direction dependent hybridization arising from the spin-orbit coupling [2], among other factors. These multiferroic systems exhibit fascinating multiferroic phenomena and magnetoelectric (ME) domain dynamics in which the specific spin pattern of $3d$-magnetic ion is mainly responsible for creating electric dipole moments

---

*Contact author: tathamay.basu@rgipt.ac.in

(i.e., nonzero polarization) [2,8,15–18]. For example, the electric polarization in well-known multiferroic compounds, such as $RMnO_3$, RMn_2O_5, $RCrTiO_5$, R_2BaNiO_5, $Ba_3NiNb_2O_9$, $CuCrO_2$, $Co_4Nb_2O_9$, and Ca_3CoMnO_6, arises from canted spin structure of $3d$-magnetic ion (Co, Mn, Ni, Cr, etc.) due to inverse DM interaction mechanism or from collinear spin-structure $3d$-magnetic ion due to the exchange-striction mechanism, or due to p-d hybridization [1,2,6,11,14]. The rare-earth (R) ions might have a key role in the resulting overall magnetic structure of $3d$ transition-metal ions on these systems, but spins of R ions are not directly involved in the mechanism of spin-driven ferroelectricity. For example, in the well-known $RMnO_3$ compound, the noncollinear structure of Mn gives rise to polarization due to inverse DM interaction, where the R ion has an indirect role in the Mn-spin pattern [1,2]. However, the spin-driven polarization arising from inverse DM interaction between two different magnetic species has rarely been reported. A little theoretical study exists on this aspect [9,19,20], but experimental reports are rare in this aspect. For the magnetoelectric compound $NdCrTiO_5$, theoretical studies suggest that the spin-driven polarization emerges due to inverse DM interaction between noncollinear spins of both Cr and Nd [20]; however, there is no experimental evidence of this spin structure. The significant role of both Tb and Ni spins (noncollinear spins) on magnetoelectric coupling is also predicted theoretically for the multiferroic compound Tb_2BaNiO_5, although no clear mechanism is demonstrated [9]. For the well-known multiferroic series RMn_2O_5, the compound $GdMn_2O_5$ shows much larger polarization compared to other R members [4,5]. It is described that in addition to the Mn-Mn exchange-striction, the exchange-striction of Gd-Mn (collinear spins) contributes to the net ferroelectric polarization, yielding a larger polarization in this compound when compared with the remaining members of the family [4,19]. In this study, both spins of transition metal (d) and rare earth (f) directly take part in breaking the inversion symmetry. Moreover, all these studies are restricted to $3d$ transition metal [9,19–22]. The search for potential multiferroic material in the hybrid metal-organic network has been explored as well, where magnetodielectric coupling is documented but spin-driven ferroelectricity is not demonstrated [23–25]. Recently, the search for potential multiferroic materials was extended to strongly correlated $4d/5d$ orbital systems to investigate the nature of ME coupling. The pronounced effect of stronger spin-orbit coupling, the larger radial extension of d orbital, and the crystal-field effect in $4d/5d$ orbital, when compared to that of $3d$ orbital, is considered crucial in magnetism, multiferroicity, and thus ME coupling. For example, a stronger spin-orbit coupling may help to enhance the ME coupling strength through inverse DM interaction, whereas the crystal field could have a significant effect in deciding the magnetic ground state as well as lattice distortion. However, the larger extension of the $4d/5d$ orbitals, when compared to that of $3d$, makes the sample less insulating and hinders the experimental determination of the polarization. Therefore, despite strong theoretical prediction [26], experimental reports of $4d/5d$- (non-d^0)-based multiferroic (spin-driven ferroelectric) compounds are rare. Very recently, magnetodielectric coupling and multiferroicity were experimentally demonstrated in a $4d$-$4f$ coupled system,

$Ba_3HoRu_2O_9$ [27–29], which has increased research activities in this field searching for $4d$ transition-metal oxide-based multiferroic systems. Further investigations are warranted to understand the mechanism of the (magnetism-driven) ferroelectricity, which has not yet been explored.

Another interesting area is the effect of external parameters (e.g., pressure, magnetic field) on multiferroicity. These have a huge influence on spin and dipoles resulting in distortion in lattice and change in superexchange magnetic interaction, which varies with rare-earth metal, even in the same series due to competing magnetic interactions. For example, an interesting reentrant multiglass behavior below the multiferroic ordering temperature is observed in the Haldane-chain system R_2BaNiO_5, in which the external magnetic field has an intriguing effect [15,16,30]. The magnetic and dielectric ordering both shift to lower temperature under the application of magnetic field for the compound Er_2BaNiO_5 [15], whereas the dielectric peak shifts in the opposite direction compared to that of magnetic feature in the presence of magnetic field for the isostructural Dy_2BaNiO_5—-an observation that still requires further investigation [16]. A large enhancement of pressure-induced multiferroicity (ordering temperature or/and value of electric polarization) by stabilizing the magnetic phase-competing ground state has been theoretically predicted in many multiferroic systems (e.g., CuO, $PbCoO_3$) [29–32]. However, the corresponding experimental realization is very limited (e.g., $GdMn_2O_5$, $PrMn_2O_5$, and Mn_2GeO_4) [19,33,34].

The compound that is at the center of this paper, $Ba_3HoRu_2O_9$, crystallizes in a *6H* perovskite structure and consists of Ru_2O_9 dimers (face-sharing distorted RuO_6 octahedral) and regular corner-sharing RO_6 octahedral (Fig. 1) [29,35]. This system undergoes an antiferromagnetic ordering at $T_{N2} \sim 10.2$ K. The magnetic superexchange interaction develops through the path "Ru-O-Ho-O-Ru" (Fig. 1). It is demonstrated that magnetodielectric (MD) coupling is stronger for heavy rare-earth members [29]. Among all the known compositions, $Ba_3HoRu_2O_9$ exhibits the strongest MD coupling and shows ferroelectricity with a weak polarization value below the magnetic ordering ($T_{N2} = 10.2$ K) [29]. Our recent neutron-diffraction studies [27] reveal that the compound $Ba_3HoRu_2O_9$ exhibits magnetic ordering at $T_{N1} = 50$ K, associated with a propagation wave vector of $k_1 = (0.5 \ 0 \ 0)$, followed by another magnetic phase transition around $T_{N2} = 10.2$ K that results in a more complex magnetic phase. In contrast, other members studied in this family (R = Tb, Gd, Er, Sm, etc.) until now have shown only the low-temperature antiferromagnetic ordering ($\sim$10–12 K) [27,29,35], except $Ba_3NdRu_2O_9$, which has shown ferromagnetic ordering at 24 K (where Nd moments order), followed by another ordering at 17 K (Ru moments also order), where Ru_2O_9-dimers order antiferromagnetically [36]. Interestingly, for our titled compound $Ba_3HoRu_2O_9$, both Ru and Ho-moments order simultaneously below T_{N1}, followed by spin reorientations at lower temperatures, revealing a strong Ru ($4d$)-Ho ($4f$) magnetic coupling in this system [27]. Below T_{N2}, in addition to a sharp reorientation of Ho- and Ru spin moments, another magnetic phase with a propagation wave vector $K_2 = (0.25 \ 0.25 \ 0)$ emerges and coexists with the one associated with k_1, revealing a competing magnetic ground
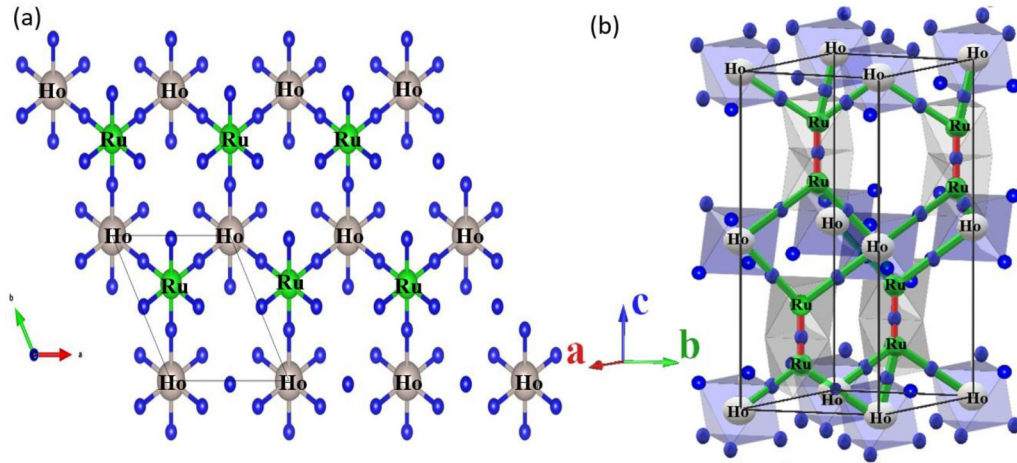
FIG. 1. Crystal structure of $Ba_3HoRu_2O_9$ [green (Ru), gray-white (Ho), and blue (oxygen)]; Ba atoms are removed for a clear view to show superexchange path. (a) in *ab* plane, and (b) 3D view to show the HoO_6 and RuO_6 octahedra and Ru-O-Ru superexchange path (in red) and Ho-O-Ru superexchange path (in green).

state [27]. The second magnetic phase is characterized by an up-up-down-down ($\uparrow\uparrow\downarrow\downarrow$) spin structure of each Ru- and Ho spin. The compound exhibits a peak in the *T*-dependent complex dielectric constant at the onset of the second magnetic phase transition (T_{N2}), which has a pronounced effect in the presence of a magnetic field, mimicking the magnetic feature observed in magnetic susceptibility and heat capacity [29]. This confirms magnetodielectric coupling. Further, positive-up-negative-down (PUND) ferroelectric polarization measurements at 5 K (below T_{N2}) confirm the ferroelectricity characterizing this compound as multiferroic [29].

However, it is not clear how spin drives the ferroelectric polarization. The studies presented here contribute to the understanding of the nature of magnetic ordering and spin dynamics around T_{N2} and, consequently, elucidate the mechanism of magnetoelectric coupling and multiferroicity in this compound. We have demonstrated that inverse DM interaction between Ru ($4d$) and Ho ($4f$) spins related to the spin structure of the second magnetic phase transition breaks the inversion symmetry, producing nonzero electric polarization. In addition, we have studied the effect of external pressure. Our results suggest that external pressure enhances the magnetic ordering, probably by reducing the magnetic phase competition.

II. EXPERIMENTAL DETAILS

The powder sample $Ba_3HoRu_2O_9$ was synthesized by solid-state reaction using mixtures of high-purity (>99.9%) precursors: $BaCO_3$, RuO_2, and Ho_2O_3, which were mixed in an agate mortar and pestle and pressed into pellets as described in Refs. [29,35] The compound formed a single phase with $P6_3/mmc$ space group as reported earlier [29,35].

Temperature-dependent ac magnetic susceptibility measurements were carried out using a Quantum Design superconducting quantum interference device (SQUID). The high-pressure SQUID measurement was done using a beryllium copper homemade clamp-style cell in Oak Ridge National Laboratory (ORNL). The sample magnetization is

calculated by subtracting the empty pressure-cell data. The ambient-pressure (standard sample loading) dc magnetization is conducted in the presence of 100–50-kOe magnetic field in zero-field-cooled (ZFC) mode (the sample is cooled under zero field from paramagnetic region to 2 K and then the magnetic field is applied; the data has been taken during warming) and after that, the dc magnetization is taken under 10-kOe magnetic field applying different pressure (0–1.2 GPa) in the same ZFC mode.

The complex dielectric measurements as a function of temperature, magnetic field, and frequency (1-V ac bias, 1–100 kHz) were performed using an Impedance analyzer (Agilent 4284A). This measurement setup is integrated to a Quantum Design physical properties measurement system. Silver paint was used to make parallel-plate capacitors of the pressed disklike polycrystalline samples.

Neutron powder-diffraction patterns were collected at the SNAP beamline, a time-of-flight diffractometer dedicated to high-pressure research at Spallation Neutron Source, Oak Ridge Laboratory, USA. To cover the regions of interest in reciprocal space the detector banks were placed at a central scattering angle of 50° and 65° about the sample in the scattering plane (each spanning a 45° range) and two central wavelengths selected were 2.4 and 6.4 Å, leading to an incident beam with usable wavelength spectra of 0.65–4.15 Å, and 4.65–8.15 Å (second frame). The resulting diffraction data covered a range in momentum transfer Q from 0.9–10 Å^{-1} or, in d spacing, from 0.5 Å < d < 7 Å. In the second frame, the corresponding ranges are momentum transfer Q from 0.4−1.8 Å^{-1} or, in d, spacing from 3.5 Å < d < 12 Å. The available low-Q range in time-of-flight neutron-diffraction measurement will be able to track any other magnetic peak (if one appears) for both propagation vectors k_1 and k_2.

The sample was placed in a liquid He-cooled wet "orange" cryostat and data were collected from room temperature down to 4 K. Two sets of measurements were attempted: one at ambient pressure where the sample was loaded on a thin-walled 6-mm-diameter vanadium can, and another set using a high-strength CuBe clamp pressure cell 10 mm in diameter.

Initial analysis indicated that the elevated background levels of the relatively smaller amounts of sample measured and the weak magnetic scattering in the pressure cell precluded the tracking of the magnetic phases with pressure. As such, in the following, only the ambient pressure data are presented.

We have carried out the temperature-dependence high-resolution x-ray diffraction (HRXRD) on the CRISTAL beamline in SOLEIL synchrotron (France) with an x-ray source of wavelength $\lambda = 0.58182$ Å.

III. RESULTS AND DISCUSSION

A. Time-of-flight neutron diffraction and mechanism of spin-driven ferroelectricity

Here, we will elucidate the mechanism of spin-driven polarization. To confirm the magnetic structure, we have performed neutron diffraction at SNAP (ORNL), which allowed us to measure the low-Q regime to detect all the magnetic peaks of both magnetic phases associated with $K_1(0.5\ 0\ 0)$ and $K_2(0.25\ 0.25\ 0)$, as shown in Fig. 2(a). We have reproduced the same spin structure as obtained in our earlier paper [27]. The spin structure shown in Figs. 3(a) and 3(b) are associated with k_1 and k_2 wave vectors at 4 K.

The electric polarization in this system most likely may arise through inverse Dzyaloshinskii-Moriya interactions from noncollinear magnetic structure (spin-current model) or through exchange-striction from the collinear spin structure. First, we have calculated inverse DM interaction [$P_{ij} \propto e_{ij} \times (S_i \times S_j)$] between nearest Ru- and Ho spins (Ru-O-Ho configurations) of magnetic phase related to k_1-spin structure, shown in Fig. 3(c) for $T = 4$ K. This results in local polarization; however, the direction of the polarization of one Ru-O-Ho configuration is opposite the neighboring configuration. Hence, the net polarization is canceled out in the whole magnetic unit cell (in macroscopic scale), as shown in Fig. 3(c). We have also calculated the same at $T = 30$ K (not shown here), which does not yield any macroscopic polarization as well. Therefore, the inverse DM interaction associated with noncollinear k_1-spin structure cannot produce ferroelectric polarization. The system magnetically orders below 50 K (T_{N1}) associated with k_1-spin structure. The absence of ferroelectricity in $T_{N1} < T < T_{N2}$ agrees with the above conclusion. The clear peak in dielectric constant is observed at T_{N2} and ferroelectricity is observed below T_{N2}, where second magnetic phase related to k_2-spin structure emerges. Initially, it was assumed that the spin-driven ferroelectricity might arise from exchange-striction of ↑↑↓↓ spin structure of Ho or Ru from second magnetic phase, similar to that observed in the Ca_3CoMnO_6 system [14]. In the exchange-striction mechanism, the symmetric exchange interaction between the parallel spins (↑↑ or ↓↓) helps to make a shorter bond which moves the ion closer; subsequently, opposite (antiparallel) spins (↑↓) make the bond longer between these two ions, which creates a local polarization. Here, the exchange interaction is mediated via oxygen ions. For ↑↑↓↓-spin structure (k_2) in ab plane of this compound, the Ho ions are connected to next Ho ions via Ho-O-Ru-O-Ho exchange-path or via Ho-O-Ba-O-Ho path (see Fig. 1); therefore, no Ho-O-Ho path exists. Thus, the superexchange interaction between two nearest Ho spins is
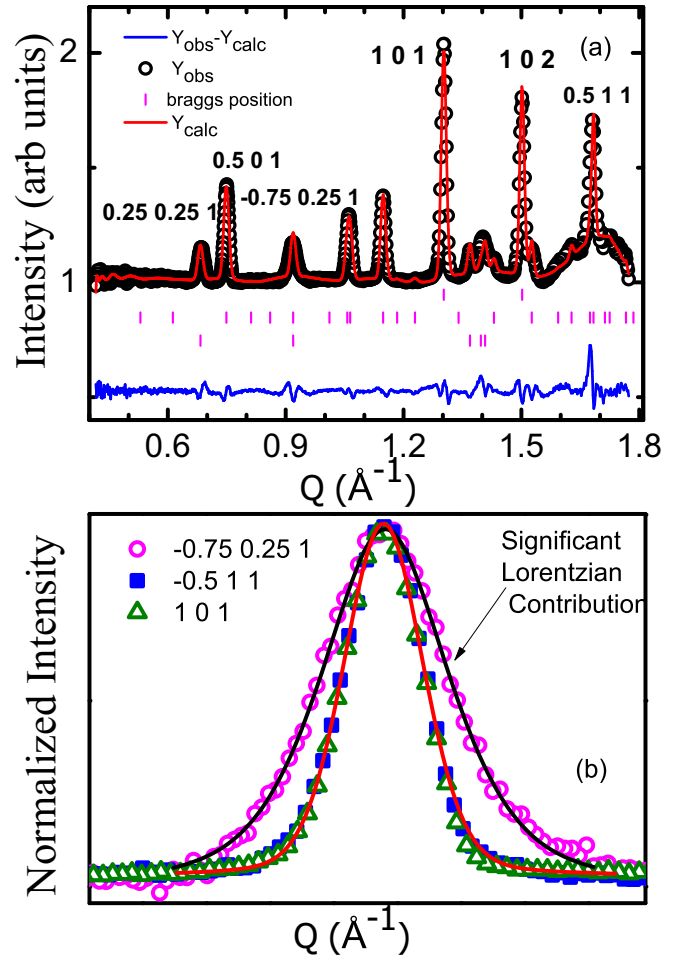

FIG. 2. (a) Rietveld refinement of time-of-flight neutron-diffraction data in the low-Q regime at $T = 4$ K of $Ba_3HoRu_2O_9$. The open black circle represents the experimental data, while the red solid line shows the Rietveld fitting. The vertical bars display the Bragg peak positions: The upper vertical lines are Bragg lines for the crystal structure, followed by reflections associated with $k_1 = (0.5\ 0\ 0)$ and $k_2 = (0.25\ 0.25\ 0)$, respectively. The lower blue line is the difference between the experimental and calculated intensity (b) Normalized peaks for lattice (1 0 1), k_1 (0.5 1 1), and k_2 (−0.75 0.25 1) magnetic structure as discussed in the text. The value of the x axis (Q) is shifted for each plot to place the peak at the same position to compare the peak shape directly. The solid line is fitting of these peaks. The solid red line is fitted with Gaussian and the solid black line is fitted with Gaussian and Lorentzian parameters.

not possible; the superexchange path should be via Ru (see Fig. S1 in Supplemental Material (SM) [37]). Hence, ↑↑↓↓ Ho spins cannot have such exchange-striction effect (negligible displacement) and such a configuration cannot produce any polarization. The Ru-O-Ru superexchange interaction is restricted in Ru_2O_9 dimers, as they are not directly interconnected (a clear view is shown in Fig. S1 in SM [37]). The magnetic ordering is obtained via Ru-O-Ho exchange path only. Therefore, the exchange-striction mechanism in ↑↑↓↓ spin structure of only Ho- or Ru ions cannot produce dipole moment. In ↑↑↓↓ (k_2)-spin-structure, the individual Ru-spin moments or individual Ho-spin moments are collinear
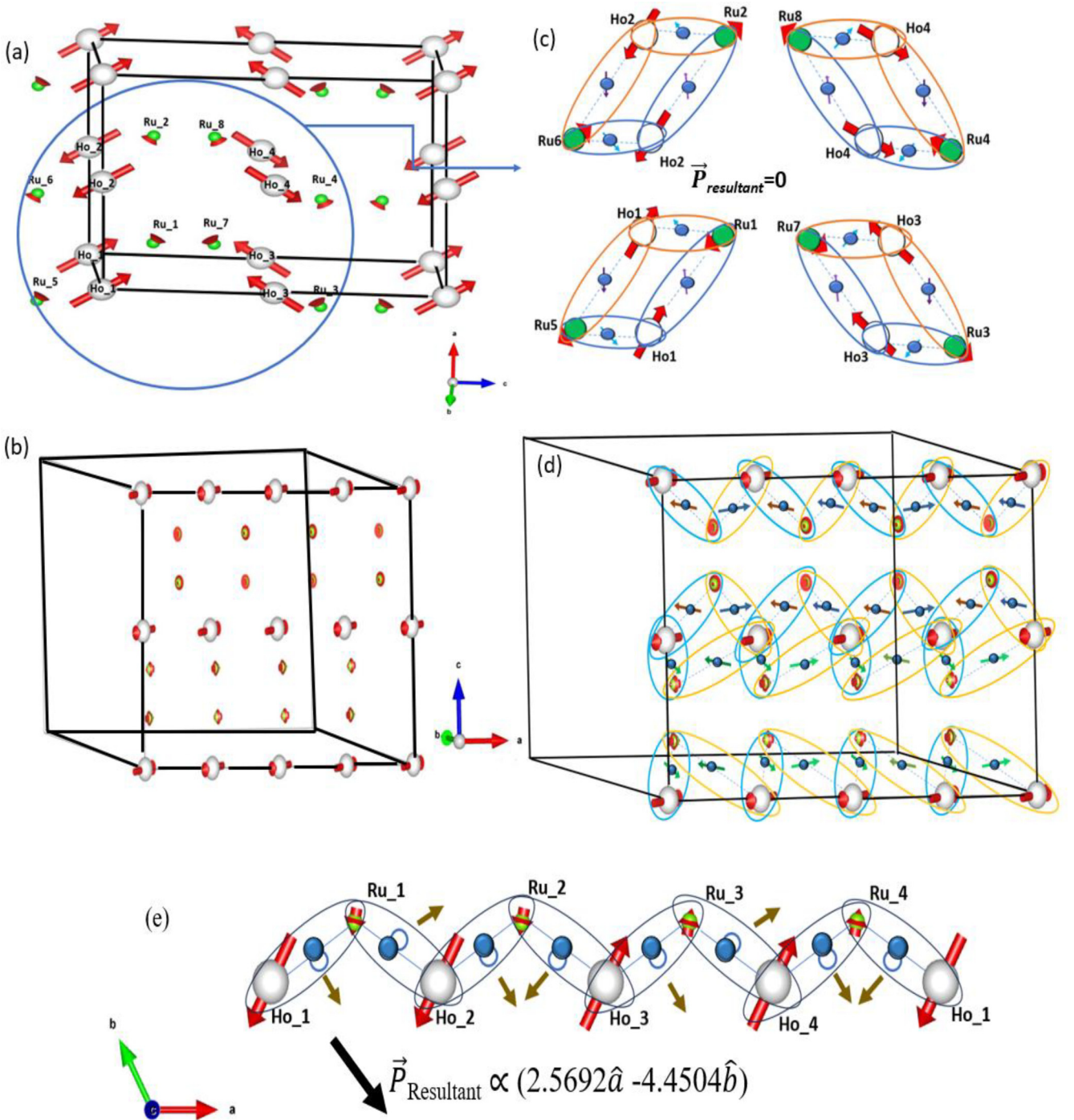
FIG. 3. Magnetic structure of (a) first magnetic phase (canted structure) associated with k_1-wave vector, and (b) second magnetic phase (up-up-down-down structure) associated with k_2-wave vector at $T = 4$ K for $Ba_3HoRu_2O_9$. The oxygen atoms in between Ru and Ho atoms are not shown in the figure. (c), (d) Calculated inverse DM interaction considering all neighboring Ru- and Ho spins for each structure, respectively, as discussed in the text. The atoms are denoted in a different color as follows: white (Ho), green (Ru), and blue (oxygen). The red arrow on Ho and Ru atoms denotes the spins of the respective atoms. The arrow on oxygen shows the direction of local polarization, that is, the direction of inverse DM interaction between related Ho and Ru spins of corresponding Ho-O-Ru configuration. The large black arrow shows the direction of resultant polarization. The resultant polarization is zero for (c) and nonzero for (d). (e) The spin structure and displacement of oxygen atoms due to inverse DM interaction between Ho and Ru spins are schematically shown. The displacement of oxygen atoms (closed blue circle) is schematically depicted with open blue circle, which is along the direction of inverse DM interaction (shown with a brown arrow). The resultant polarization (that is proportional to inverse DM interaction) does not cancel out in the macroscopic scale, shown with a large black arrow. The detailed calculation is described in SM [37].

in the *ab* plane among themselves; nevertheless, the Ho- and Ru spins are noncollinear to each other (connected via Ru-O-Ho-O-Ru exchange path) even in the *ab* plane (see Fig. S1 in SM [37]). The Ru-O-Ho-O-Ru superexchange paths are shown in Fig. 1 and Fig. 3(d), where Ho- and Ru ions are arranged in a zigzag pattern. The presence of larger *d* orbitals (4*d*) results in strong spin-orbit coupling in this system. Normally, stronger spin-orbit coupling may favor the DM interaction, which may lead to a preference for non-collinear spin configurations of Ho and Ru via strong *d-f* coupling. In this study, we observed a low magnetic moment of the Ru atom, which was 1.1 μ_B compared to its average spin-only values in Ru^{4+} (d^4) and Ru^{5+} (d^3) states. This observation further suggests the possibility of electron itineracy with a larger extension of 4*d* orbital, or/and competing effects of crystal-field effects and spin-orbit coupling of the Ru atom in this system. We have calculated the inverse DM interaction between the nearest Ru and Ho (connected via Ru-O-Ho path) of this (k_2)-spin-structure, which produced a nonzero value that shifted the oxygen atoms and thus, nonzero local polarization [see Figs. 3(d) and 3(e)]. We have calculated for the whole unit cell. We obtained that the local polarization did not cancel out in the whole unit cell and a nonzero resultant polarization was obtained in the *ab* plane [Figs. 3(d) and 3(e)]. The detailed spin structure in different orientations (Fig. S2) and calculation of inverse DM interaction [$P_{ij} \propto e_{ij} \times (S_i \times S_j)$] are clearly documented in SM [37].

To date, there are mostly experimental reports of those multiferroic compounds where spin pattern of 3*d*-metal ion is responsible for spin-driven ferroelectricity, as discussed in the Introduction. However, the experimental evidence of electric polarization as a result of inverse DM interaction of noncollinear spin moments occurring between two different atoms does not exist. The multiferroic $GdMn_2O_5$ compound exhibits the largest polarization among all multiferroic-II compounds (that is, multiferroic magnetoelectric system where spin drives the ferroelectricity). It is demonstrated that the exchange-striction mechanism between collinear spins of Gd (4*f*) and Mn (3*d*) contributed to a larger polarization of $GdMn_2O_5$ compound [19]. Here we observed that the spin-driven polarization was governed from noncollinear spin-structure of two different atoms, that is, Ho (4*f*) and Ru (4*d*) through inverse DM interaction. This further supports strong 4*d*-4*f* correlation in this system. The stronger spin-orbit coupling in larger 4*d* orbital compared to that of 3*d* orbital might play a decisive role.

B. Magnetoelectric domain dynamics

The polarization through PUND measurement was reported to be very low [29]. To understand this behavior, we have investigated the spin and dipolar domain dynamics of the $Ba_3HoRu_2O_9$ compound through combined dielectric characterization, ac magnetic susceptibility, and neutron time-of-flight measurements. We have measured the dielectric constant as a function of temperature in the absence magnetic field at various frequencies from $\nu = 1.1-120$ kHz, which is shown in Fig. 4. The low-frequency data below 1 kHz could not be recorded due to the low signal-to-noise ratio.
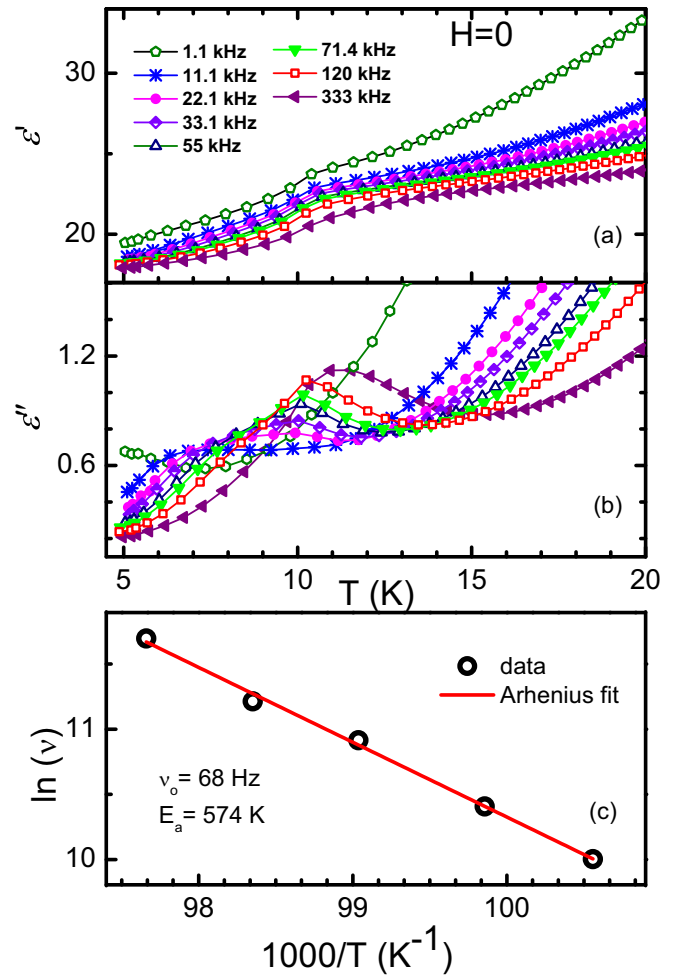

FIG. 4. (a) The real and (b) imaginary part of dielectric constant as a function of temperature under various frequencies (1.1–120 kHz). (c) Arrhenius plot ln ν vs inverse of T_p. The low-frequency data in (c) are not included either due to absence of the corresponding peak or very broad features.

The real (ε') and imaginary (ε'') parts of the dielectric constant are presented in Figs. 4(a) and 4(b). The dielectric peak appears at the onset of magnetic ordering T_{N2} as a result of strong magnetodielectric coupling, as reported earlier. Interestingly, the peak present in $\varepsilon'(T)$ and $\varepsilon''(T)$ exhibits a frequency-dependent behavior around T_{N2}. The peak temperature (T_P) of $\varepsilon'(T)$ and $\varepsilon''(T)$ shifts to a higher temperature with increasing frequency (ν). Figure 4(c) shows the plot of ln(ν) versus the inverse of T_p (peak temperature extracted from ε''), showing it follows an Arrhenius relation [$\nu = \nu_0 \exp (E_a/k_B T_p)$, $\nu_0 =$ preexponential factor, and $E_a =$ activation energy], exhibits logarithmic relaxation behavior with $E_a \sim 574$ K. The frequency-dependence behavior can be observed due to the presence of dipolar glass behavior or ferroelectric domain relaxation/ reorientation. These results combined with ac susceptibility and neutron results (discussed below) indicate the presence of finite-size ferroelectric domains in this compound. The activation energy is related to the energy barriers associated with the ferroelectric domain reorientation. Very low polarization
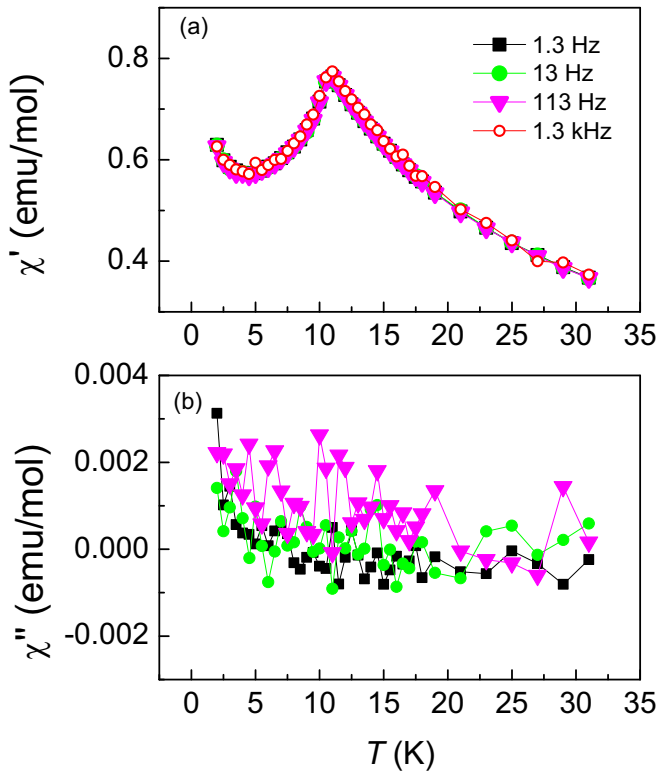
FIG. 5. (a) The real part (χ') and (b) imaginary part (χ'') of ac magnetic susceptibility as a function of temperature for various frequencies from 1.3 Hz–1.3 kHz.

value in PUND measurement is consistent with the concept of finite-size ferroelectric (magnetoelectric) domains instead of true long-range ordering. A similar effect was reported in the well-known multiferroic compound Ca_3CoMnO_6, where a low polarization value was experimentally obtained due to the finite-size domains instead of true long-range ordering [14].

The ac magnetization as a function of temperature is shown in Fig. 5 for different frequencies (1 Hz–1.3 kHz), which does not yield any frequency-dependence behavior, in contrast with the dielectric constant. We propose this could be an artifact arising from a different frequency regime in which the finite-size magnetic domains respond to higher frequencies. Similar behavior is observed in the magnetism-driven ferroelectric system Dy_2BaNiO_5, where the frequency-dependent behavior is observed only in high-frequency regions (>10 kHz) [16]. The response of the finite-size magnetic domains can be very weak for low-frequency regions.

We have analyzed the peak shape in neutron diffraction to clearly resolve this issue. We have superimposed three normalized representative peaks obtained from neutron diffraction in Fig. 2(b). We have considered the different peaks at $T = 4$ K; one is (1 0 1) peak for the nuclear structure (only lattice Bragg peak), the other one is (-0.5 1 1) peak, which is a magnetic peak related to k_1-spin structure ($k_1 = 0.5$ 0 0), and the third one is (-0.75 0.25 1) magnetic peak for k_2-spin structure (magnetic Bragg peak related to $k_2 = 0.25$ 0.25 0). The ($- < 0.511$) magnetic peak related to the k_1-spin structure is well fitted with the (Gaussian) peak-shape parameters same as the (1 0 1) lattice peak used in the refine-

ment [Fig. 2(b)]. The (-0.75 0.25 1)-peak shape associated with the k_2-spin structure shows significant broadening when compared to that of the k_1-spin structure [see Fig. 2(b)]. One needs to introduce significant Lorentzian parameters to fit the peaks associated with k_2-spin structure. Therefore, we only observe the broadening of the magnetic peak related to k_2-spin structure; no broadening is observed for the magnetic peak associated with k_1-spin structure even at low temperature below T_{N2}. This shows that the k_2-spin structure has a shorter coherence length compared to that of k_1-spin structure and it arises through the development of finite-size magnetic domains. This result, together with our frequency dependence magnetic and dielectric results, predicts the magnetoelectric domain dynamics.

These results clearly support our electric polarization model, where spin-driven ferroelectric polarization arises from the k_2-spin structure; however, the net polarizations (of a domain) nearly cancel out due to random domain dynamics of magnetoelectric domains in bulk macroscopic scale yielding very weak experimentally observed polarization. In this structure, the spins are oriented with ↑↑↓↓-spin structure of Ho- and Ru spins individually and noncollinear between Ho- and Ru spins. A higher magnetic field may destabilize the spin structure, where spins will try to reorient along the applied H. Eventually, a spin can be flipped (↑↑↑↓) by changing the whole spin structure, depending on the strength of the magnetic field. The H-induced magnetic transition ~ 36 kOe and the $M(T)$ feature at a very high field (50 kOe) are consistent with such behavior [19]. If there is a change of spin pattern, then definitely the canting angle of Ru and Ho spins will be different; therefore, the direction of the vector $[\mathbf{e}_{ij} \times (\mathbf{S}_i \times \mathbf{S}_j)]$ will be different. The relative spin orientation between S_{Ru} and S_{Ho} under a high magnetic field is such that overall polarization may cancel out on a macroscopic scale. The shifting of the dielectric peak towards lower temperature with increasing magnetic field, and further the suppression (absence) of the dielectric feature under the high magnetic field of 50 kOe [29], is consistent with this (spin-driven) ferroelectric polarization model.

C. Influence of external pressure

The external parameters (e.g., field, pressure, etc.) have a strong effect on the magnetic (multiferroic) ordering of material. Earlier, we observed that the application of a magnetic field decreases the ordering temperature as observed from the shifting of T-dependence magnetic and dielectric peak towards low temperature with increasing magnetic field and a very high magnetic field (say, $H = 50$ kOe) destroys the multiferroicity [29], consistent with our spin-driven ferroelectric model. Here, we investigate the effect of another parameter, that is, external pressure on the magnetic (multiferroic) ordering of this system. The dc magnetic susceptibility (M/H) under different magnetic fields is shown in Fig. 6(a). Temperature-dependent magnetization shows a peak at ~ 10.2 K as reported in the literature [29,35]. This peak shifts to a lower temperature and broadens with an increasing magnetic field, eventually being suppressed at 50 kOe, agreeing with the previous report [29]. This result confirms the reproducibility of the magnetic feature where the pressure cell does not have
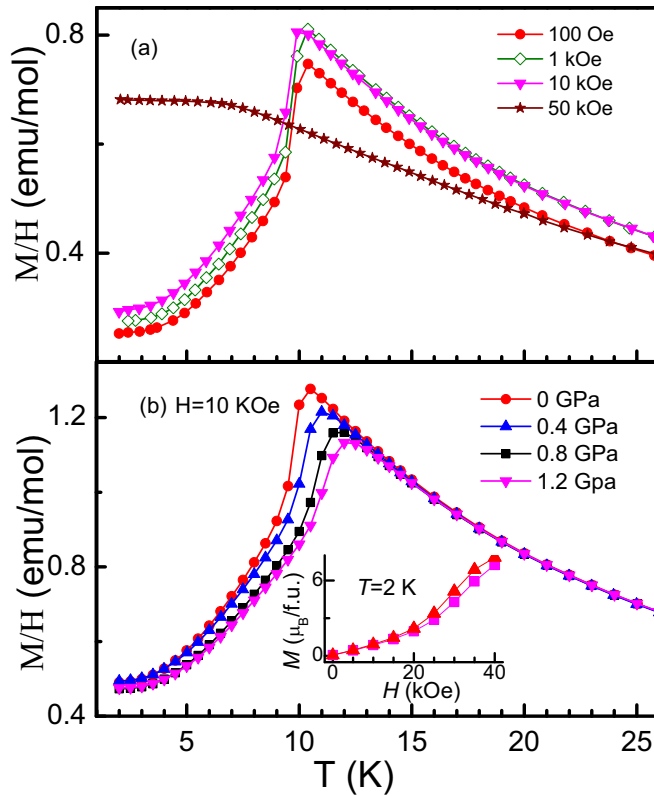
FIG. 6. dc magnetic susceptibility as a function of temperature: (a) in different applied field for zero applied pressure, and (b) under different applied pressures (0, 0.4, 0.8, and 1.2 GPa) in the presence of 10-kOe magnetic field. The inset of (b) shows the isothermal magnetization $M(H)$ in the absence of pressure and the presence of 1.2-GPa pressure.

FIG. 7. Synchrotron powder x-ray-diffraction pattern of $Ba_3HoRu_2O_9$ (a) at 8 K and (b) 80 K for space group (SG) 194, and (c) synchrotron powder x-ray-diffraction pattern of $Ba_3HoRu_2O_9$ at 8 K for SG 190 in Rietveld refinement.

any extrinsic effect on the measurements. We have plotted the dc magnetization under external pressure at a fixed magnetic field of 10 kOe in Fig. 6(b). Interestingly, the temperature of the magnetic peak increases with increasing external pressure. The magnetic peak at 10.2 K in the absence of external pressure shifts to 11, 11.5, and 12.2 K under the application of small pressure of 0.5, 0.8, and 1.2 GPa, respectively, corresponding to an enhancement of ~1.6 K/GPa. These results suggest that external pressure and magnetic field have opposing effects on the magnetic ordering temperature. The inset of Fig. 6(b) shows the isothermal magnetization plot as a function of the magnetic field for the absence and presence of external pressure of 1.2 GPa at $T = 2$ K. We observe a small decrease in the magnetization value at 2 K in $M(H)$ under external pressure, which is consistent with $M(T)$ behavior.

In the well-known spin-driven ferroelectric system, $DyMn_2O_5$, the application of pressure enhances the ferroelectric polarization at low temperatures by stabilizing the commensurate Mn-spin order [24]. In $RMnO_3$ (R = Dy, Tb, and Gd), the system was found to show a pressure-induced phase transition into the phase with large spin-driven ferroelectric polarization along the "*a*" axis [25]. Density-functional simulations suggest that the enhancement of polarization by applying pressure in $TbMnO_3$ is due to the stabilization of a collinear up-up-down-down spin-ordered state [25]. Here, we speculate that similarly to previous
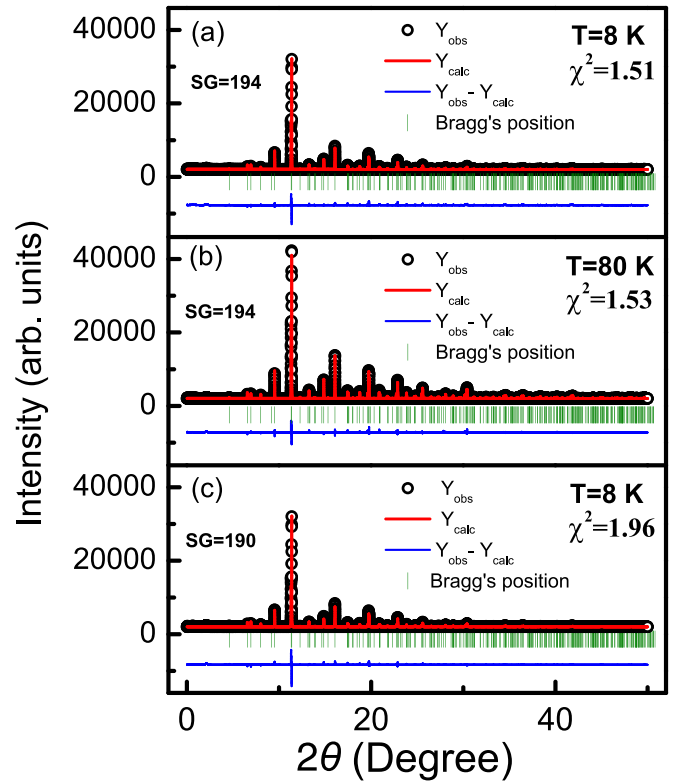
reports on other systems, pressure (mildly) stabilizes the up-up-down-down, structure resulting in an enhancement of magnetic ordering competing with temperature fluctuations.

As mentioned earlier, attempts were made to collect neutron diffraction under external pressure, but the weak neutron transmission through the cell body, along with aspects discussed in the earlier experimental section, precluded the collection of usable data for structural and magnetic refinements.

D. Temperature-dependence x-ray diffraction

We have analyzed the synchrotron high-resolution powder XRD data using Rietveld refinement [38] in the temperature range of 4–300 K. The Rietveld refinement fitting of HRXRD data at 8 and 80 K is shown in Fig. 7. We observed that the crystal symmetry remains consistent in temperature fitting with $P6_3/mmc$ (194) space group. The T-dependence plot of lattice parameters (a, c) is represented in Figs. 8(a) and 8(b) from 4–40 K. [39,40] A clear anomaly in the lattice parameters (a, c) around the transition temperature T_{N2} is observed.

Cooling from the high temperature, the lattice constants (a, c) reduce with decreasing temperature due to thermal contraction. However, at the onset of the T_{N2}, the curve goes upward for lattice constant "c" with the decreasing temperature, which is not usual. The lattice constant a also shows a peak at T_{N2}. The change in the lattice volume (V) with temperature is shown in Fig. 8(c), which displays a clear anomaly around
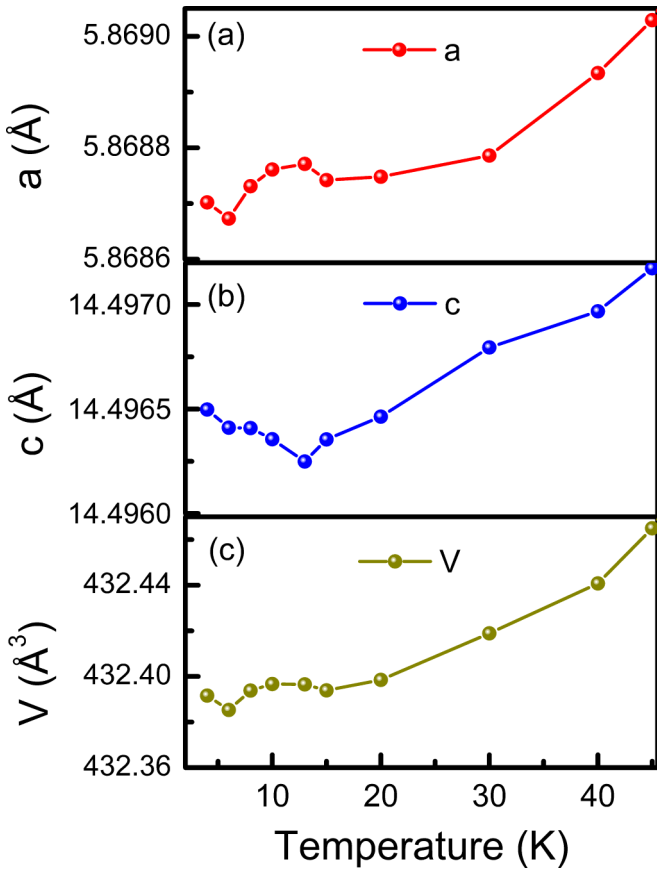
FIG. 8. (a), (b) Thermal variation of lattice parameters (*a*- and *c* axes), respectively. (c) Thermal variation of lattice volume. The symbol size represents the error of the data.

T_{N2} in the form of a peak. Considering that lattice volume is directly linked to the Gibbs free energy (*G*), $V = (\frac{\partial G}{\partial P})_T$, any discontinuity in volume implies a discontinuity in Gibbs free energy. This observation indicates a possible first-order type phase transition. [41] A sharp change in *T*-dependence heat capacity is observed at T_{N2}, predicting the first-order nature of the phase transition [27], consistent with this result.

We have also checked some other noncentrosymmetric space groups related to this structure (where spatial inversion symmetry is broken), although, we did not find any further improvement in the goodness of fit with these related space groups. We have analyzed the XRD data with a noncentrosymmetric space group with a similar structure. The Rietveld refinement fitting at $T = 8$ K for the noncentrosymmetric space group, $P\bar{6}2c$, is shown in Fig. 7(c). We found equally good fitting for both the space groups at 8 K. It is to be noted that the displacement of atoms in multiferroic-II (spin-driven ferroelectric) is generally too small to be traced in the x-ray/neutron diffraction. Until now, for all the reported spin-driven ferroelectric systems, the breaking of spatial inversion symmetry is not traceable directly from the XRD analysis; rather, an anomaly in the lattice parameters around multiferroic ordering is reported in the literature [27,41,42]. Friedel's law states that the intensities of the *h, k, l* and −*h,* −*k,* −*l* reflections are equal. This is true if the crystal is centrosymmetric or if no resonant scattering is present.

It is impossible to conclude by x-ray powder diffraction whether an inversion center is present unless significant structural change is there in general. Combining the results of synchrotron x-ray and bulk ferroelectric measurements, we propose the noncentrosymmetric space group $P\bar{6}2c$ for this title compound.

IV. CONCLUSION

We have investigated in detail the mechanism of spin-driven electric polarization on $Ba_3HoRu_2O_9$, an ideal model for a 4*d*-4*f* coupled system, through dielectric spectroscopy, magnetization measurements, time-of-flight neutron diffraction, and temperature-dependent synchrotron x-ray diffraction. The ferroelectricity below T_{N2} arises from inverse DM interaction between the noncollinear moments of Ho- and Ru-magnetic ions of second magnetic phase related to k_2-spin structure, where each Ho and Ru spin forms a collinear ↑↑↓↓ spin structure but Ho and Ru ions are noncollinear connected via Ru-O-Ho exchange path. This is an experimental demonstration of spin-driven ferroelectricity in a 4*d*-4*f* system; not only that, spin-driven polarization, arising due to inverse DM interaction of two different magnetic ions [here, Ho (4*f*) and Ru (4*d*)], is rarely (experimentally) demonstrated in any *d-f* system. Only for the well-known multiferroic $GdMn_2O_5$ compound (which is considered to be one of the best spin-driven ferroelectric compounds in which the largest polarization is observed among multiferroic-II systems), it is demonstrated that the exchange-striction mechanism between collinear spins of Gd (4*f*) and Mn (3*d*) takes part in contributing to larger polarization. The weak polarization observed in our titled compound $Ba_3HoRu_2O_9$ is attributed to the partial cancellation of magnetoelectric domains, as estimated from the excess broadening of on second magnetic phase (k_2-spin structure) in the neutron diffraction. The clear anomaly in the lattice parameters and volume obtained from high-resolution synchrotron XRD results also supports the ferroelectric phase transition at T_{N2}. Our synchrotron XRD results propose a noncentrosymmetric space group ($P\bar{6}2c$) for this compound. An application of a very high magnetic field destroys such spin structure and thus ferroelectricity. Interestingly, the application of external pressure has an opposite effect on the magnetic ordering (T_{N2}) compared to the external magnetic field. The application of 1.2-GPa pressure enhances the magnetic ordering T_{N2} by 2 K. Other microscopic experiments, such as μSR spectroscopy and polarized neutron diffraction [43] under extreme condition, are warranted for further understanding the spin dynamics of $Ba_3HoRu_2O_9$. Our results hopefully motivate further investigations on 4*d* − 4*f* coupled systems where the magnetic phase might be stabilized and may yield a large polarization.

[1] T. Kimura, T. Goto, H. Shintani, K. Ishizaka, T. Arima, and Y. Tokura, Magnetic control of ferroelectric polarization, Nature (London) **426**, 55 (2003).

[2] Y. Tokura, S. Seki, and N. Nagaosa, Multiferroics of spin origin, Rep. Prog. Phys. **77**, 076501 (2014).

[3] V. Balédent, S. Chattopadhyay, P. Fertey, M. B. Lepetit, M. Greenblatt, B. Wanklyn, F. O. Saouma, J. I. Jang, and P. Foury-Leylekian, Evidence for room temperature electric polarization in RMn$_2$O$_5$ multiferroics, Phys. Rev. Lett. **114**, 117601 (2015).

[4] N. Lee, C. Vecchini, Y. J. Choi, L. C. Chapon, A. Bombardi, P. G. Radaelli, and S.-W. Cheong, Giant tunability of ferroelectric polarization in GdMn$_2$O$_5$, Phys. Rev. Lett. **110**, 137203 (2013).

[5] G. R. Blake, L. C. Chapon, P. G. Radaelli, S. Park, N. Hur, S.-W. Cheong, and J. Rodríguez-Carvajal, Spin structure and magnetic frustration in multiferroic RMn$_2$O$_5$ (R = Tb,Ho,Dy), Phys. Rev. B **71**, 214402 (2005).

[6] T. Basu, D. T. Adroja, F. Kolb, H.-A. Krug von Nidda, A. Ruff, M. Hemmida, A. D. Hillier, M. Telling, E. V. Sampathkumaran, A. Loidl, and S. Krohns, Complex nature of magnetic field induced ferroelectricity in GdCrTiO$_5$, Phys. Rev. B **96**, 184431 (2017).

[7] J. Hwang, E. S. Choi, H. D. Zhou, J. Lu, and P. Schlottmann, Magnetoelectric effect in NdCrTiO$_5$, Phys. Rev. B **85**, 024415 (2012).

[8] K. Singh, T. Basu, S. Chowki, N. Mahapotra, K. K. Iyer, P. L. Paulose, and E. V. Sampathkumaran, Magnetoelectric coupling in the Haldane spin-chain system Dy$_2$BaNiO$_5$, Phys. Rev. B **88**, 094438 (2013).

[9] R. Kumar, S. Rayaprol, S. Rajput, T. Maitra, D. T. Adroja, K. K. Iyer, S. K. Upadhyay, and E. V. Sampathkumaran, Existence of a critical canting angle of magnetic moments to induce multiferroicity in the Haldane spin-chain system Tb$_2$BaNiO$_5$, Phys. Rev. B **99**, 100406(R) (2019).

[10] F. Kagawa, S. Horiuchi, M. Tokunaga, J. Fujioka, and Y. Tokura, Ferroelectricity in a one-dimensional organic quantum magnet, Nat. Phys. **6**, 169 (2010).

[11] A. Maignan *et al.*, Fe$_2$Co$_2$Nb$_2$O$_9$: A magnetoelectric honeycomb antiferromagnet, J. Mater. Chem. C **9**, 14236 (2021).

[12] P. Šenjug, J. Dragović, F. Torić, I. Lončarić, V. Despoja, K. Smokrović, E. Topić, I. Đilović, M. Rubčić, and D. Pajić, Magnetoelectric multiferroicity and magnetic anisotropy in guanidinium copper (II) formate crystal, Materials **14**, 1730 (2021).

[13] J. Wang, X. L. Xu, and X. A. Li, Recent progress of multiferroicity and magnetoelectric effects in ABX$_3$-Type perovskite metal–organic frameworks, Adv. Mater. Interfaces **10**, 2300123 (2023).

[14] Y. J. Choi, H. T. Yi, S. Lee, Q. Huang, V. Kiryukhin, and S.-W. Cheong, Ferroelectricity in an Ising chain magnet, Phys. Rev. Lett. **100**, 047601 (2008).

[15] T. Basu, K. Singh, N. Mohapatra, and E. V. Sampathkumaran, Magnetic and dielectric behavior of the spin-chain compound Er$_2$BaNiO$_5$ well below its Néel temperature, J. Appl. Phys. **116**, 114106 (2014).

[16] T. Basu, P. L. Paulose, K. K. Iyer, K. Singh, N. Mohapatra, S. Chowki, B. Gonde, and E. V. Sampathkumaran, A reentrant phenomenon in magnetic and dielectric properties of Dy$_2$BaNiO$_5$ and an intriguing influence of external magnetic field, J. Phys.: Condens. Matter **26**, 172202 (2014).

[17] A. M. Kadomtseva, S. S. Krotov, Yu. F. Popov, and G. P. Vorob'ev, Features of the magnetoelectric behavior of the family of multiferroics RMn$_2$O$_5$ at high magnetic fields (review), Low Temp. Phys. **32**, 709 (2006).

[18] K. Singh, A. Maignan, D. Pelloquin, O. Perez, and C. Simon, Magnetodielectric coupling and magnetization plateaus in α-CoV$_2$O$_6$ crystals, J. Mater. Chem. **22**, 6436 (2012).

[19] L. H. Yin, D. H. Jang, C. B. Park, K. W. Shin, and K. H. Kim, Pressure-induced ferroelectricity and enhancement of Mn-Mn exchange striction in GdMn$_2$O$_5$, J. Appl. Phys. **119**, 104101 (2016).

[20] S. Kori, T. Okamura, R. Okazaki, I. Terasaki, and Y. Yasui, Anomalous magnetic order in the magnetoelectric oxide NdCrTiO$_5$ revealed by impurity effects, Phys. Rev. B **91**, 144403 (2015).

[21] J. Song, B. Zhao, L. Yin, Y. Qin, J. Zhou, D. Wang, W. Song, and Y. Sun, Reentrant spin glass behavior and magnetodielectric coupling of an Ir-based double perovskite compound, La$_2$CoIrO$_6$, Dalton Trans. **46**, 11691 (2017).

[22] M. Čebela, D. Zagorac, I. Popov, F. Torić, T. Klaser, Ž. Skoko, and D. Pajić, Enhancement of weak ferromagnetism, exotic structure prediction and diverse electronic properties in holmium substituted multiferroic bismuth ferrite, Phys. Chem. Chem. Phys. **25**, 22345 (2023).

[23] T. Basu, C. Bloyet, F. Beaubras, V. Caignaert, O. Perez, J.-M. Rueff, A. Pautrat, B. Raveau, J.-F. Lohier, P.-A. Jaffrès, H. Couthon, G. Rogez, G. Taupier, and H. Dorkenoo, Designing of a magnetodielectric system in hybrid organic–inorganic framework, a perovskite layered phosphonate MnO$_3$PC$_6$H$_4$-m-Br · H$_2$O, Adv. Funct. Mater. **29**, 1901878 (2019).

[24] Y. Tian, S. Shen, J. Cong, L. Yan, S. Wang, and Y. Sun, Observation of resonant quantum magnetoelectric effect in a multiferroic metal–organic framework, J. Am. Chem. Soc. **138**, 782 (2016).

[25] T. Basu, A. Jesche, B. Bredenkötter, M. Grzywa, D. Denysenko, D. Volkmer, A. Loidl, and S. Krohns, Magnetodielectric cou-

pling in a non-perovskite metal–organic framework, Mater. Horiz. **4**, 1178 (2017).

[26] M. Ležaić and N. A. Spaldin, High-temperature multiferroicity and strong magnetocrystalline anisotropy in 3d-5d double perovskites, Phys. Rev. B **83**, 024410 (2011).

[27] T. Basu, V. Caignaert, F. Damay, T. W. Heitmann, B. Raveau, and X. Ke, Cooperative Ru(4d)-Ho(4f) magnetic ordering and phase coexistence in the 6H perovskite multiferroic Ba$_3$HoRu$_2$O$_9$, Phys. Rev. B **102**, 020409(R) (2020).

[28] T. Basu, A. Pautrat, V. Hardy, A. Loidl, and S. Krohns, Magnetodielectric coupling in a Ru-based 6H-Perovskite, Ba$_3$NdRu$_2$O$_9$, Appl. Phys. Lett. **113**, 042902 (2018).

[29] T. Basu, V. Caignaert, S. Ghara, X. Ke, A. Pautrat, S. Krohns, A. Loidl, and B. Raveau, Enhancement of magnetodielectric coupling in 6H-perovskites Ba$_3$RRu$_2$O$_9$ for heavier rare-earth cations (R = Ho,Tb), Phys. Rev. Mater. **3**, 114401 (2019).

[30] K. K. Iyer, R. Kumar, S. Rayaprol, K. Maiti, and E. V. Sampathkumaran, Pressure-induced anomalies in the magnetic transitions of the exotic multiferroic material Tb$_2$BaNiO$_5$, Phys. Rev. Mater. **5**, 084401 (2021).

[31] F. Lou, W. Luo, J. Feng, and H. Xiang, Genetic algorithm prediction of pressure-induced multiferroicity in the perovskite PbCoO$_3$, Phys. Rev. B **99**, 205104 (2019).

[32] X. Rocquefelte, K. Schwarz, P. Blaha, S. Kumar, and J. van den Brink, Room-temperature spin-spiral multiferroicity in high-pressure cupric oxide, Nat. Commun. **4**, 1 (2013).

[33] W. Peng *et al.*, Toward pressure-induced multiferroicity in PrMn$_2$O$_5$, Phys. Rev. B **96**, 054418 (2017).

[34] T. Honda *et al.*, Pressure effect on magnetism and multiferroicity in Mn$_2$GeO$_4$, Phys. Rev. B **89**, 104405 (2014).

[35] Y. Doi and Y. Hinatsu, Magnetic and calorimetric studies on Ba$_3$LnRu$_2$O$_9$(Ln = Gd, Ho–Yb) with 6H-perovskite structure, J. Mater. Chem. **12**, 1792 (2002).

[36] M. S. Senn, S. A. J. Kimber, A. M. Arevalo Lopez, A. H. Hill, and J. P. Attfield, Spin orders and lattice distortions of geometri-

cally frustrated 6H-perovskites Ba$_3$B′Ru$_2$O$_9$ (B′ = La^{3+}, Nd^{3+}, and Y^{3+}), Phys. Rev. B **87**, 134402 (2013).

[37] See Supplemental Material at http://link.aps.org/supplemental/ 10.1103/PhysRevB.109.224418 for the detailed calculation of the mechanism of spin-driven ferroelectric polarization and spin structure in different planes. Figure S1 shows the lattice structure along with spin patterns related to the k_2-spin structure of Ba$_3$HoRu$_2$O$_9$ in the ac plane. Figure S2 shows the inverse DM interaction between Ru and Ho spins, which is mediated via intermediate O atoms in the $> ac$ plane and ab plane.

[38] J. Rodríguez-Carvajal, Recent advances in magnetic structure determination by neutron powder diffraction, Physica B **192**, 55 (1993).

[39] K. Sun, Y. Zhu, S. Wu, J. Xia, P. Zhou, Q. Zhao, and H. F. Li, Temperature-dependent structure of an intermetallic ErPd$_2$Si$_2$ single crystal: A combined synchrotron and in-house X-ray diffraction study, Powder Diffr. **37**, 91 (2022).

[40] S. Mathew, A. R. Abraham, S. Chintalapati, S. Sarkar, B. Joseph, and T. Venkatesan, Temperature dependent structural evolution of WSe$_2$: A synchrotron X-ray diffraction study, Condensed Matter **5**, 76 (2020).

[41] M. Numan, G. Das, M. S. Khan, G. Manna, A. Banerjee, S. Giri, and S. Majumdar, Evidence of exchange striction and charge disproportionation in the magnetoelectric material Ni$_3$TeO$_6$, Phys. Rev. B **106**, 214437 (2022).

[42] T. Basu, V. R. Kishore, S. Gohil, K. Singh, N. Mohapatra, S. Bhattacharjee, and E. V. Sampathkumaran, Displacive-type ferroelectricity from magnetic correlations within spin-chain, Sci. Rep. **4**, 5636 (2014).

[43] J. Stein, S. Biesenkamp, T. Cronert, T. Fröhlich, J. Leist, K. Schmalzl, and M. Braden, Combined Arrhenius-Merz law describing domain relaxation in Type-II multiferroics, Phys. Rev. Lett. **127**, 097601 (2021).